

## Elasticity and modal effects on the optimal performance of micro-perforated multi-layered absorbers

Cédric Maury<sup>1</sup>

Laboratory of Mechanics and Acoustics (LMA CNRS UMR 7031)

4 impasse Nikola Tesla, 13013 Marseille, France

Teresa Bravo<sup>2</sup>

Institute for Physical and Information Technologies (ITEFI)

Spanish National Research Council (CSIC)

Serrano 144, 28006 Madrid, Spain

### ABSTRACT

*Multi-layered wall-treatments with thin lightweight micro-perforated panels offer a potential solution to achieve broadband noise absorption while complying with mass saving and compactness. This study examines how vibrational effects, often neglected, may impede the wideband acoustical performance of such partitions, made up of a distribution of either periodic or graded micro-perforated membranes or panels. The impedance translation method and a scattering matrix analysis have been implemented. It is found that the elasticity behavior of thin micro-perforated membranes has a beneficial effect on the acoustical efficiency of the partitions. The contributions of the individual acoustical resonances tend to merge if the elasticity effects are accounted for. If the partition is optimized, near-constant high absorption and low transmission values are obtained over a wide frequency range. A more robust design involves partitions made up of micro-perforated panels. It was observed that the first volumetric mode of the panels degrades the absorption properties of the partition. It cross-couples with the acoustical resonances and redistributes their spectral locations. This structural resonance sets a lower frequency bound, above which the partition can achieve a high broadband performance. It should be accounted for when setting the frequency limits of the total dissipation to be optimized.*

### 1. INTRODUCTION

Partitions made up of Micro-Perforated Panels (MPPs) are porous solutions able to achieve noise absorption or insulation in the mid-frequency range and under severe environments, without particle emissions while complying with lightweight and space constraints. Practical developments include the design of fan casings lined with microperforated absorbers [1], but also the development of space sound absorbers [2] to improve speech intelligibility in noisy room environments. These single or multi-resonant absorbers are composed of thin panels with sub-millimetric holes or slits separated by air cavities. A proper optimization of their constitutive parameters (holes diameter, perforation ratio, thickness, cavity depth) may substantially enhance their acoustical dissipative performance and broaden their efficiency range towards low frequencies [3,4].

---

<sup>1</sup> cedric.maury@centrale-marseille.fr

<sup>2</sup> teresa.bravo@csic.es

In the context of acoustic metamaterials, it was shown that multi-layered partitions made up of identical perforated panels with super-millimetric hole diameters, and separated by air gaps of sub-wavelength thickness, the so-called acoustic fishnets, exhibit stop-band transmission properties over specific tunable frequency bands [5,6]. Downshift and broadening of the stop-bands can be achieved when considering equally-spaced identical MPPs [7], with however substantial transmission over the first pass-band at low frequencies and significant reflections over the transmission stop-bands.

In order to achieve both low reflection and transmission, functionally-graded porous materials have been designed with suitable chirped variations of their parameters in order to produce full dissipation of the incident energy over a broad bandwidth [8,9]. Their design is based on the critical coupling condition, that monitors the visco-thermal losses so that they exactly balance the amount of reflection and transmission leakages [10]. For instance, a serial distribution of chirped Helmholtz resonators, with gradual axial variation of their cavity depths, enabled to achieve broadband unit dissipation [8].

In this work, the acoustical properties of acoustic fishnets as well as functionally-graded (micro-)perforated partitions (FGMPP) are examined. In the latter case, the idea is to progressively decrease the porosity of the panels from the front to the back side in order to achieve both impedance matching and suitable merging of the hole-cavity resonances over a broad bandwidth. Of interest is to assess how the vibrational effects of the thin constitutive micro-perforated panels or membranes may modify these properties and how to optimize their performances by accounting for vibrational effects.

Comparatively, there is a fewer amount of studies that account for vibrational effects in MPP partitions, often assumed to be made of rigid panels. For instance, the absorption peaks induced by the flexural vibrations of a finite-sized flexible circular MPP have been analytically described [11]. The effects of the coupled structural and acoustic resonances were examined in order to broaden the absorption bandwidth of rigidly-backed flexible MPP absorbers [12,13]. Of interest was to elucidate how the micro-perforations modify the modal behavior of a membrane and monitor the relative amount of energy structurally or acoustically dissipated [14]. A Finite Element Method (FEM) enabled to assess the effects of boundary conditions on the transfer impedance of a flexible MPP system [15]. The effective transfer impedance that accounts for dissipative and inertial effects across the apertures of a single rigid MPP is described by well-established formulations [16,17]. It has been extended towards thin elastic limp micro-perforated membranes assuming continuity of the air-particle velocity at the perforation boundary [18]. Additional structural damping induced by the micro-perforations has been modelled with maximum effect at a characteristic frequency that depends on the perforation ratio [19].

The current study examines how the vibrational effects may impede or enhance the acoustical performance of optimized acoustic fishnet and FGMPP partitions. Section 2 presents extended formulations for the MPP transfer impedance that incorporate elasticity or modal effects. Section 3 examines how these effects influence the dissipation, reflection, transmission and input impedance of acoustic fishnets. Section 4 analyzes from a critical coupling approach the resonance performance of FGMPPs whose total dissipation has been optimized over a broad bandwidth. Section 5 resumes the main results and proposes follow-ups.

## 2. EXTENDED IMPEDANCE FORMULATIONS

The acoustical performance of multi-layered partitions made up of  $Q$  equally-spaced rigid or elastic MPPs are modelled from the impedance translation approach. A double-layered partition with  $Q = 3$  is sketched in Figure 1. The MPPs of thickness  $t_q$  are characterized by their holes diameter  $d_{h,q}$  and their center-to-center holes separation distance  $\Lambda_{h,q}$ , so that the

perforation ratio reads  $\sigma_{h,q} = \pi d_{h,q}^2 / (4\Lambda_{h,q}^2)$  for aligned holes. The MPPs are separated by  $(Q-1)$  air layers of constant depth  $D_q = D$ .

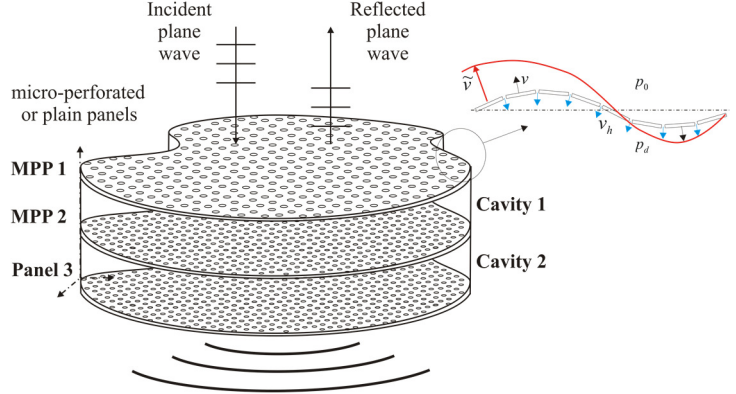


Figure 1: (left) Photography of a partition made up of thin micro-perforated panels; (right) sketch of a double layered graded micro-perforated partition with elasticity effects illustrated in the inset.

The MPP holes diameter stay constant, say  $d_{h,q} = d_h$ , across the acoustic fishnet made up of identical panels. However, one assumes that the holes diameters of the FGMP partition regularly decrease from the front to the back panel, according to the law  $d_{h,q+1} = d_{h,q} - \beta_q \Lambda_{h,q} / 2$  ( $q = 1, \dots, Q$ ) with  $\beta_q$  a tunable rate of decay for the holes diameter. The front panel is excited by a normal incident plane wave while the back panel radiates a plane wave in free-field.

The impedance translation approach (ITA) provides a recursive relationship for the effective input impedance of each panel-cavity layer,  $Z_{\text{input},q}$  ( $q = 1, \dots, Q-1$ ),

$$Z_{\text{input},q} = Z_{\text{MPP},q} + Z_0 \frac{Z_{\text{input},q+1} \cos(k_0 D_q) + jZ_0 \sin(k_0 D_q)}{Z_0 \cos(k_0 D_q) + jZ_{\text{input},q+1} \sin(k_0 D_q)}, \quad (1)$$

obtained from particle velocity and acoustic pressure continuity over the MPP-air layer interfaces, with  $k_0 = \omega/c_0$  the acoustic wavenumber,  $c_0$  the sound speed,  $Z_0 = \rho_0 c_0$  the air characteristic impedance,  $\rho_0$  the air density and  $Z_{\text{input},Q} = Z_{\text{MPP},Q} + Z_0$  the input impedance of the transmitting back panel. The normal incidence reflection coefficient is obtained as  $r = |(Z_{\text{input},1} - Z_0) / (Z_{\text{input},1} + Z_0)|^2$ . The transmitted power  $\tau$  reads  $|2Z_{Q/1} / (Z_{\text{input},1} + Z_0)|^2$  with  $Z_{Q/1}$  the transfer impedance across the whole partition,

$$Z_{Q/1} = Z_0 \prod_{q=1}^{Q-1} \frac{Z_0}{Z_0 \cos(k_0 D_q) + jZ_{\text{input},q+1} \sin(k_0 D_q)}. \quad (2)$$

The dissipation coefficient is given by  $1 - r - \tau$  and the Transmission Loss (TL) is defined as  $-20 \log_{10}(\tau)$ . The ITA requires knowledge of  $Z_{\text{MPP},q}$ , the transfer impedance across each MPP.

## 2.1. Rigid panel partition

One considers rigid MPPs with zero air particle axial velocity at the holes walls. The effective transfer impedance of the  $q^{\text{th}}$  MPP,  $Z_{\text{MPP},q} = (p_0 - p_d) / \sigma v_h$ , can be written as the sum of an inner term,

$$Z_{in,q} = -j\omega\rho_0 t_q \left[ \sigma_{h,q} \left( 1 - G(\text{Sh}_{h,q} \sqrt{j}) \right) \right]^{-1}, \quad (3)$$

and an outer term,

$$Z_{ext,q} = \sigma_{h,q}^{-1} \left[ \sqrt{2\eta} \text{Sh}_{h,q} / d_{h,q} - j\omega\rho_0 8d_{h,q} / (3\pi) \right], \quad (4)$$

with  $\omega$  the angular frequency,  $\text{Sh}_{h,q} = d_{h,q} \sqrt{\omega\rho_0 / (4\eta)}$  the holes Shear number,  $\eta$  the air dynamic viscosity and  $G(u) = 2J_1(u) / [uJ_0(u)]$  with  $J_1$  and  $J_0$  Bessel functions of orders 0 and 1. Eqs. (3) and (4) describe the frictional and reactive mass effects taking place respectively within and at the inlet/outlet of the MPP holes [16].

## 2.2. Elastic micro-perforated membranes

One considers limp sheet micro-perforated membranes (MPM) of infinite lateral extent. If one applies continuity at the apertures boundary between the in-hole air-particle velocity and the wall normal velocity, one obtains the following expression for the overall transfer impedance of MPMs,  $Z_{\text{MPM},q} = (p_0 - p_d) / [\sigma v_h + (1 - \sigma)v]$ , under normal incidence [18]

$$Z_{\text{MPM},q} = Z_{\text{ext},q} + \left\{ \frac{1}{Z_{\text{in},q}} + j \frac{G(\text{Sh}_{h,q} \sqrt{j})}{\omega\rho_p t_q} \right\}^{-1}, \quad (5)$$

with  $\rho_p$  the material density.

## 2.3. MPP Modal vibrating response

One now assumes that the partition is made up of simply-supported finite-sized MPPs of length  $a$  and width  $b$ . Under normal incidence, only the resonant volumetric modes of odd orders contribute to the panels structural admittance  $Y_{p,q}$ , thus yielding

$$Y_{p,q} = \frac{-j\omega}{\rho_p t_q} \sum_{\substack{m'n' \\ \text{odd}}} \frac{16}{m'^2 n'^2 \pi^4} \frac{1}{\omega_{m'n'}^2 - \omega^2 - 2j\xi_{m'n'} \omega_{m'n'} \omega}, \quad (6)$$

with  $\omega_{m'n'} = 2\pi f_{m'n'} \sqrt{(1 - \sigma_{h,q}) / [1 + (2 - 3\nu_p)\sigma_{h,q}]}$  the angular resonance frequency related to the panel mode of order  $m'n'$ ,  $f_{m'n'} = (\pi/2) \sqrt{D_p / (\rho_p t_q)} \left[ (m'/a)^2 + (n'/b)^2 \right]$  the resonance frequency of the unperforated panel and  $\xi_{m'n'}$  the corresponding modal damping factor.  $D_p$  is the panel flexural rigidity. The effect of the MPPs volumetric mode is taken into account through an extended transfer impedance,  $\tilde{Z}_{\text{MPP},q} = Z_{\text{MPP},q} (Z_{\text{MPP},q} Y_{p,q} + 1)^{-1}$ , with  $Y_{p,q}$  given by Eq. (6).

## 3. VIBRATIONAL EFFECTS

Simulations have been performed to elucidate how vibrations may modify the acoustical performance of acoustic fishnets and FGMPPs. First, one considered micro-perforated (resp. perforated) acoustic fishnets made up of  $Q = 10$  identical MPPs of thickness 0.5 mm, holes diameter 0.5 mm (resp. 2 mm), perforation ratio 0.8% (resp. 7%) separated by air gap widths  $D = 10$  mm. Figure 2 shows the effect of elastic limp MPM with density 160 kg/m<sup>3</sup> on the

dissipation, reflection, transmission and impedance matching performance of perforated and micro-perforated acoustic fishnets.

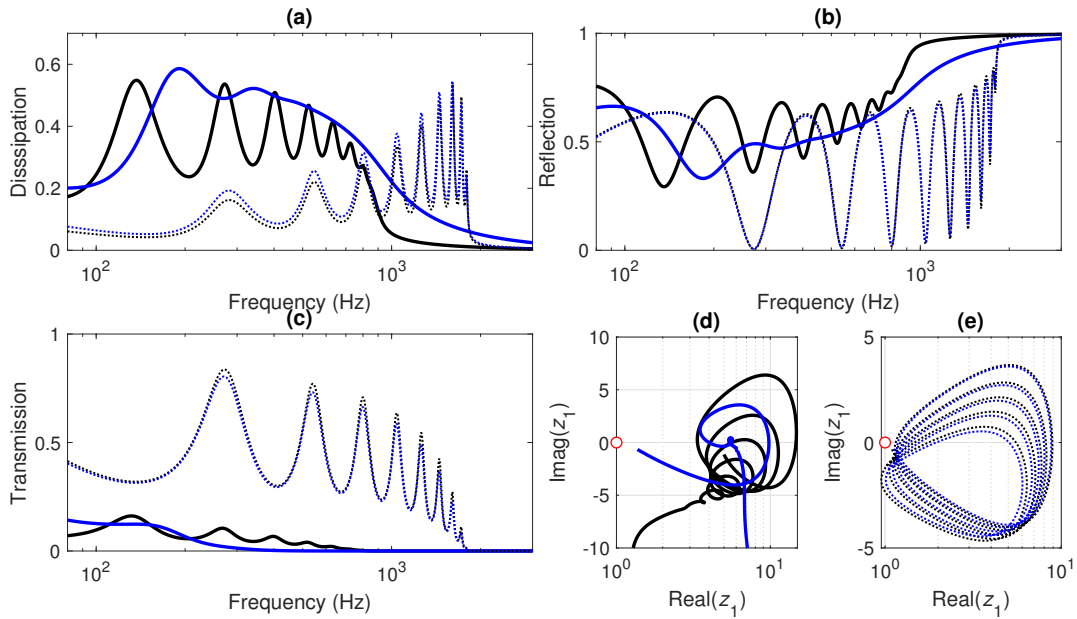


Figure 2: Elasticity effects on the dissipation (a), reflection (b), transmission (c) and specific input impedance (d-e) of an acoustic fishnet made up of 10 identical micro-perforates with holes diameter  $d_h = 0.5$  mm (thick) or  $d_h = 2$  mm (dots), assuming rigid (black) or infinite elastic membranes (blue); the red circle in (d-e) relates to impedance matching.

It can be seen from Figure 2 that the perforated acoustic fishnet exhibits a stop-band above 2 kHz with zero transmission, full reflection and zero dissipation. Below 2 kHz, hole-cavity resonances contribute to transmission and dissipation peaks related to reflection dips over the pass-band. As frequency increases, one turns from a reactive to a dissipative regime over the first pass-band. Figure 2(e) shows impedance looped curves with large radius associated to each acoustical resonance, only slightly modified by elasticity. Overall, elasticity has minute effects on the acoustical performance of the perforated fishnet. Conversely, elasticity adds overall resistance to the micro-perforated membranes. It contributes to broaden, dampen and merge the acoustical resonances that populate up to 1 kHz the pass-band of the micro-perforated acoustic fishnet. Consequently, elasticity increases the total dissipation and decreases the total reflection and transmission (although to a lesser extent) of the micro-perforated acoustic fishnet.

Second, one considered acoustic fishnets made up of finite-sized simply-supported aluminum panels of length 0.3 m, width 0.2 m and with a modal damping factor of 0.5%. One neglects the perforation ratio dependence of the added structural damping induced by the microperforations [19], but one accounts for an effective Young's modulus and density weighted by the perforation ratio (see paragraph 2.3). The panels exhibit 16 volumetric resonances up to 2.5 kHz. As for the perforated acoustic fishnet, these structural resonances appear in Figure 3 as local dissipation peaks and transmission dips as well as sub-loops of the main impedance looped curves, showing a weak coupling of the structural resonances with the hole-cavity acoustical resonances.

The structural acoustic coupling is greater when dealing with the micro-perforated acoustic fishnet, especially when the structural volumetric resonances fall within the half-bandwidth of any acoustical resonance. It produces dissipation dips followed by peaks, typical of in-phase/out-of-phase behavior of the relative airframe in-hole velocity, experimentally observed on single-layered rigidly-backed MPP partitions [20]. Overall, these resonances enhance the total dissipation and reflection performance while upshifting the acoustical

resonance frequencies, thereby enlarging the efficiency range by about 100 Hz. However, the transmission, that represents a fraction of the dissipation and reflection coefficients, is locally degraded by the structural resonances. Note that none of the acoustic fishnets, micro- or macro-perforated, achieves good impedance matching properties, as seen from Figures 2(d-e) and 3(d-e).

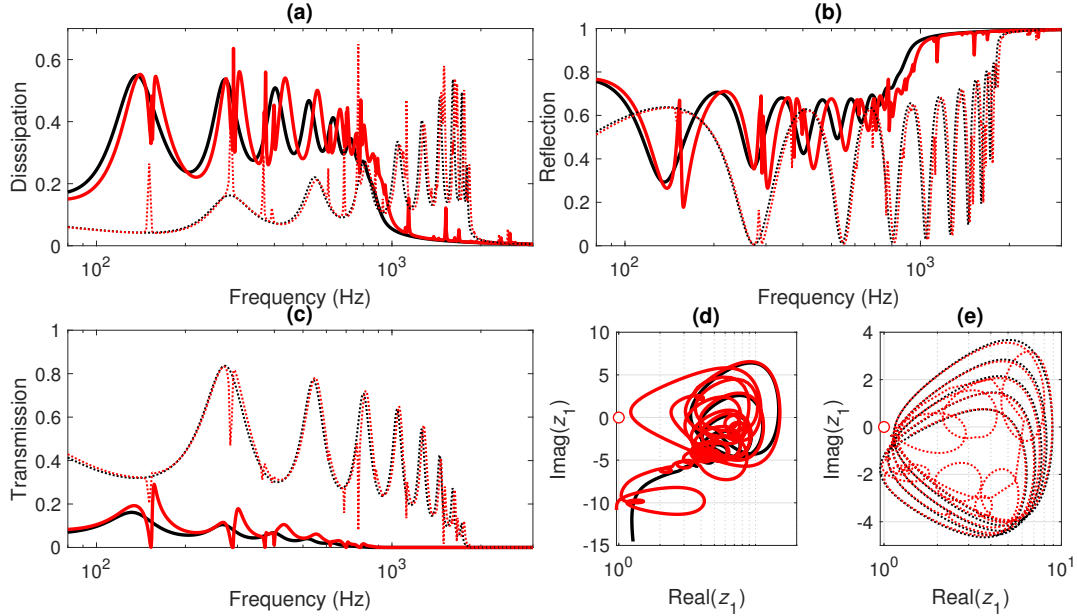


Figure 3: Effects of structural resonances on the dissipation (a), reflection (b), transmission (c) and specific input impedance (d-e) of an acoustic fishnet made up of 10 identical micro-perforates with holes diameter  $d_h = 0.5$  mm (thick) or  $d_h = 2$  mm (dots), assuming rigid (black) or finite elastic panels (red); the red circle in (d-e) relates to impedance matching.

#### 4. VIBRATIONAL EFFECTS ON OPTIMIZED MULTI-LAYERED PARTITIONS

Simulated annealing optimization of  $\beta_q$ , the holes diameter decay rate of a FGMPPs, has been achieved assuming 20 panels of thickness 0.5 mm and 1 cm holes pitch, of overall depth 30 cm separated by 1.5 cm, while maximizing the total dissipation between 100 Hz and 1 kHz.

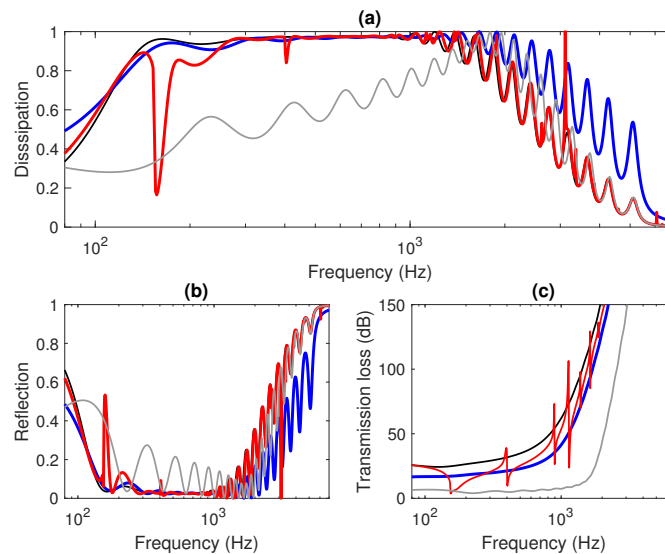


Figure 4: Vibrational effects on the dissipation (a), reflection (b) and transmission loss (c) of functionally-graded micro-perforated partitions whose total dissipation performance was maximized up to 1 kHz, assuming rigid (black), infinite elastic (blue) or finite-sized vibrating panels (red); the grey curves are related to a nominal FGMPP.

Figure 4 shows that the optimization process enabled suitable grouping and merging of the hole-cavity resonances for the rigid and MPM partitions, thereby achieving a broadband dissipation staying above 0.9 between 150 Hz and 1 kHz, as well as a reflection coefficient below 0.08 and a TL above 17 dB over this frequency range. However, it can be seen that the first volumetric resonance produces a dissipation dip down to 0.2 around 150 Hz, accompanied by a reflection peak up to 0.55 and a TL dip down to 6dB. It reduces the efficiency bandwidth of the optimized FGMPP from 100 Hz – 1 kHz to 300 Hz – 1 kHz.

Figure 5(a) shows that it is accompanied by an almost linear decay of the hole diameters from 8 mm down to 0.24 mm across the optimized rigid and modal FGMPP partitions. It can be seen from Figure 5(b) that such progressive decay achieves impedance matching conditions over the FGMPP efficiency range, conducive to efficient trapping and dissipation of the incident wave over a large bandwidth.

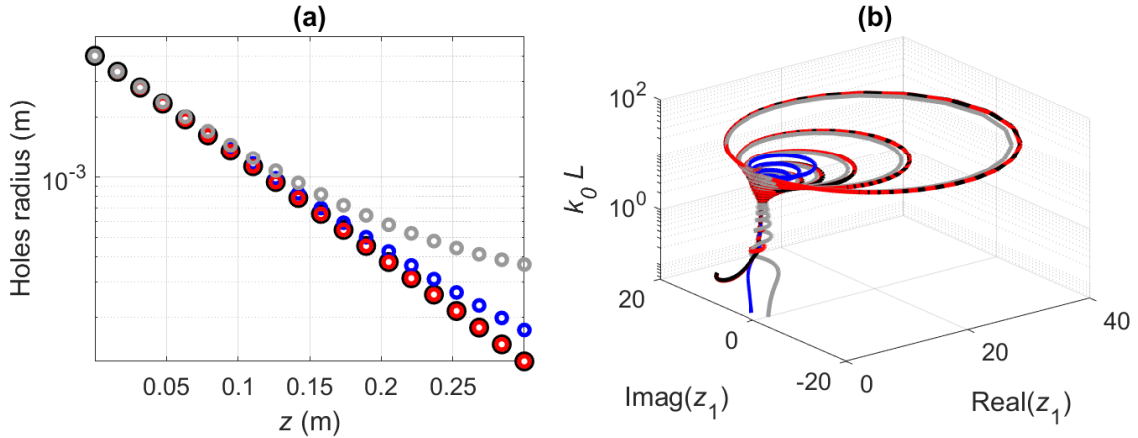


Figure 5: Vibrational effects on the holes radius distribution (a) and on the specific input impedance of functionally-graded micro-perforated partitions whose total dissipation performance was maximized up to 1 kHz, assuming rigid (black), infinite elastic (blue) or finite-sized vibrating panels (red); the grey curves are related to a nominal FGMPP.

A critical coupling analysis [10] of the scattering S-matrix that relates the outgoing and ingoing amplitudes of the two-port FGMPP partitions enables to get further insights into the resonance frequency distribution and their amount of damping required to achieve a balanced loss-to-leakage ratio. Full dissipation is achieved if the two eigenvalues of the S-matrix,  $\lambda_1$  and  $\lambda_2$ , are zero-valued for the same real frequency. Figures 6-8 show a distribution of zero-poles in the complex frequency plane ( $f_r, f_i$ ). The zeros such that  $f_i < 0$  (resp.  $f_i > 0$ ) are related to over- (resp. under-) damped resonances.

Figures 6(d-e) show that optimization of the rigid FGMPP leads to a reallocation of the hole-cavity (HC) resonances in three classes up to 2 kHz: the over-damped HC resonances below 1 kHz, critically-coupled (CC) HC resonances at 1200 Hz and 1400 Hz, and under-damped HC resonances above 1500 Hz. As for the CC resonances,  $\lambda_1$  and  $\lambda_2$  vanish at these frequencies as well as the components  $v_{11}$  and  $v_{12}$  associated to  $\lambda_1$ , indicating that an incident wave entering the FGMPP from the left is not reflected ( $R^- = 0$ ) nor transmitted ( $T = 0$ ). Although not shown,  $v_{21}$  ( $= R^+$ ) does not vanish at these frequencies, indicating that an incident wave entering the FGMPP from the right is reflected, as expected since the partition is not symmetric. It is seen in Figures 6(b-c) that the non-optimized rigid FGMPP exhibits under-damped resonances up to 1800 Hz with two CC resonances at 1820 Hz and 1960 Hz.

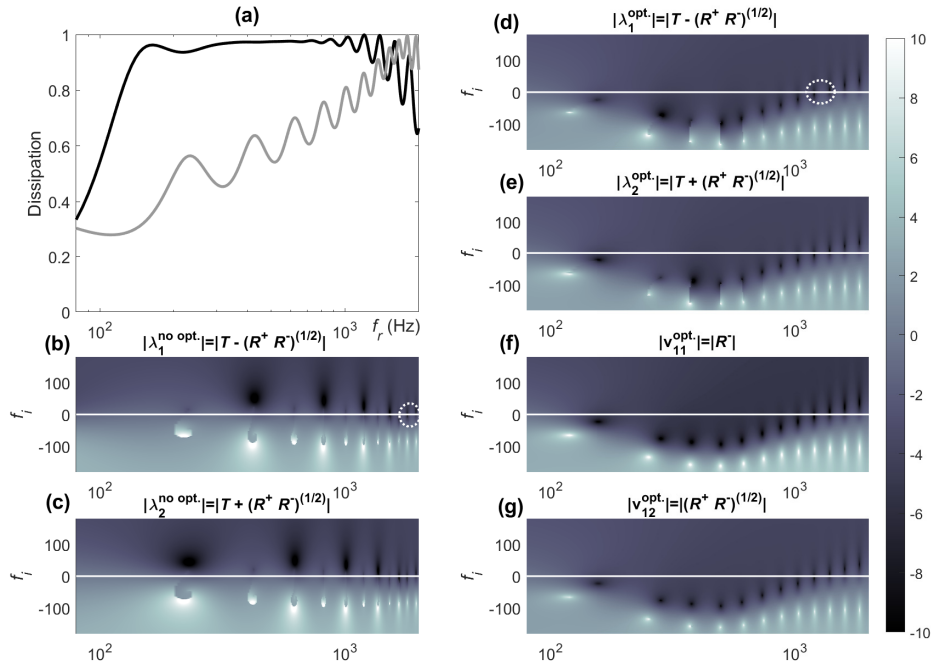


Figure 6: Effect of optimizing the total dissipation of a functionally-graded micro-perforated partition up to 1 kHz assuming rigid panels: (a) dissipation spectra (black: optimal; grey: nominal); modulus (log10 values) of the S-matrix eigenvalues in the complex frequency plane for the nominal (b, c) and optimized (d, e) FGMPs; modulus (log10 values) of the first eigenvector components for the optimized FGMP; the dotted circles spot the critically-coupled resonances;  $T$ ,  $R^-$  and  $R^+$  denote the transmission, left-to-right and right-to-left reflection coefficients.

Figure 7 shows that optimizing a partition made up of elastic limp membranes redistributes the HC resonances in two classes up to 2 kHz: a set of over-damped resonances up to 1200 Hz and three CC resonances at 1460 Hz, 1600 Hz and 1900 Hz. The optimized MPM brings additional resistance that merges the first 7 HC resonances over a larger bandwidth (up to 1200 Hz) compared to the rigid case. Moreover, the optimization process increases the number of CC resonances from one (at 1835 Hz in the nominal case) to three in the optimized case.

It can be seen from Figure 8 that the optimized performance of a vibrating FGMP assuming resonant responses of its volumetric modes substantially modifies the distribution of zero-pole pairs in the complex frequency plane. One observes up to 900 Hz a set of over-damped HC resonances that lead to high dissipation values (greater than 0.97) from 300 Hz to 900 Hz. Above the dissipation plateau, a set of CC resonances are observed between 1100 Hz and 1400 Hz, including cross-coupled Panel-Hole-Cavity (PHC) resonances at 1100 Hz and 1400 Hz. It is followed by under-damped PHC resonances up to 2 kHz.

Strong coupling between the panels' volumetric mode and the neighboring HC resonances leads to multi-resonance splitting, clearly observed in Figures 8 (d-e) at 154 Hz and 400 Hz. It is associated to an accumulation of over-damped Panel-Hole-Cavity (PHC) resonances around the panels' volumetric resonance at 154 Hz. It leads to a significant drop of the dissipated power down to 0.2 at 154 Hz, that cannot be eliminated by the optimization process. Although not shown, this drop was accompanied by an increase in the reflection up to 30% and a decrease of TL down to 6 dB.

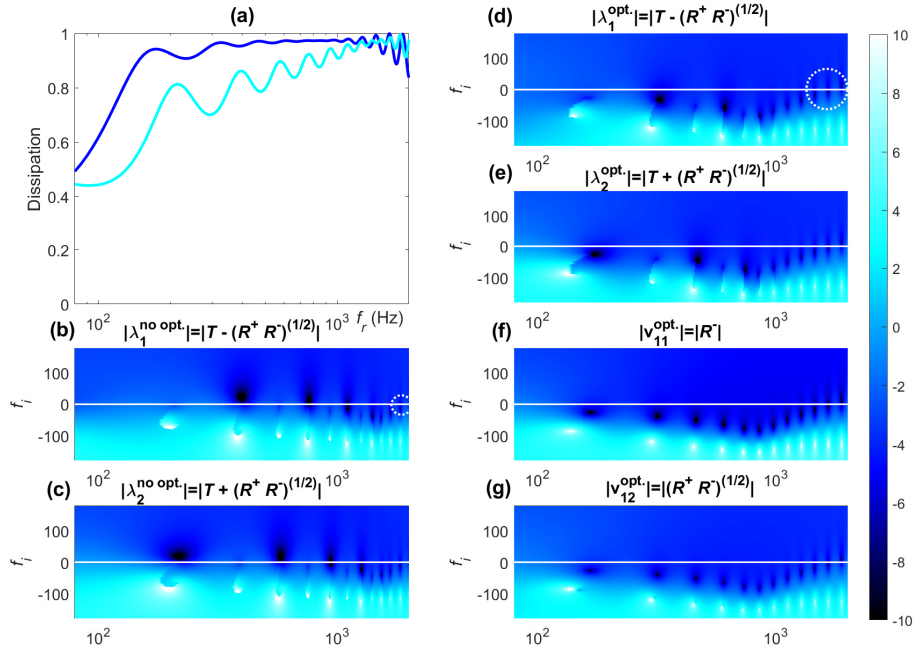


Figure 7: Effect of optimizing the total dissipation of a functionally-graded micro-perforated partition up to 1 kHz assuming infinite elastic panels: (a) dissipation spectra (blue: optimal; cyan: nominal); modulus (log10 values) of the S-matrix eigenvalues in the complex frequency plane for the nominal (b, c) and optimized (d, e) FGMPs; modulus (log10 values) of the first eigenvector components for the optimized FGMP; the dotted circles spot the critically-coupled resonances.

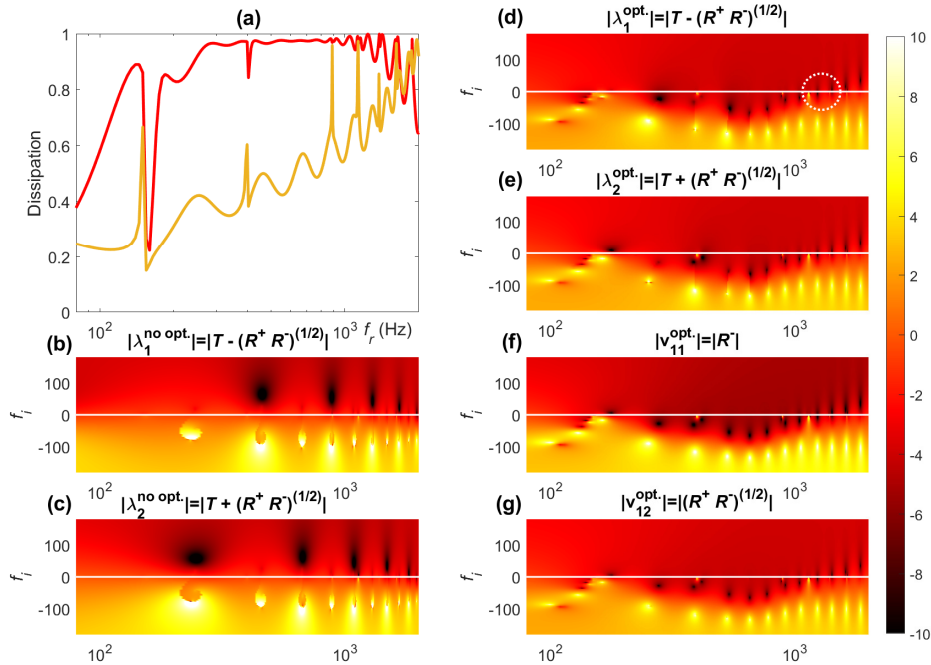


Figure 8: Effect of optimizing the total dissipation of a functionally-graded micro-perforated partition up to 1 kHz assuming finite-sized vibrating panels: (a) dissipation spectra (red: optimal; orange: nominal); modulus (log10 values) of the S-matrix eigenvalues in the complex frequency plane for the nominal (b, c) and optimized (d, e) FGMPs; modulus (log10 values) of the first eigenvector components for the optimized FGMP; the dotted circle spots the critically-coupled resonance.

## 5. CONCLUSIONS

The influence of elasticity and structural modes has been assessed on the acoustical performance of multi-layered identical or functionally-graded (micro-) perforated partitions under normal incidence from extended formulation of the translation impedance approach.

It was found that elasticity adds significant overall resistance to the micro-perforated membranes of acoustic fishnets, thereby enhancing their dissipative and reactive performance over the first pass-band. Simulated annealing optimization of the total dissipation of elastic FGMPP enabled suitable grouping and merging of the hole-cavity resonances, thereby achieving high broadband dissipation between 150 Hz and 1 kHz.

Considering multi-layered partitions with vibrating MPPs, it was shown that the panel structural volumetric resonances may strongly cross-couple with the hole-cavity resonances, thereby enhancing the total dissipation and reflection performance of acoustical fishnets. Although the optimization of structurally resonant FGMPP produces large broadband dissipation, the first panel volumetric resonance, when coupled with the neighboring hole-cavity resonances, substantially impedes the dissipation performance and reduces the FGMPP efficiency range. It produces a panel-hole-cavity resonance that sets a lower frequency bound, above which the partition can achieve a high broadband performance. It should be accounted for when setting the frequency limits for maximizing the total dissipation of a FGMPP including modal vibrational effects.

The broadband dissipation mechanism of FGMPP with gradually decaying holes diameters across the partition is reminiscent of acoustic black holes sound trapping and visco-thermal dissipation properties induced by impedance matching and progressive increase of the sidewall cavity admittances from the front to the back side. Further studies would be required to examine the analogy. Robustness of the acoustic fishnet and FGMPP acoustical properties to oblique or diffuse field incidence would also deserve attention.

## ACKNOWLEDGEMENTS

This work is part of the project TED2021-130103B-I00, funded by MCIN/AEI/10.13039/501100011033 and the European Union "NextGenerationEU"/PRTR, and project PID2022-139414OB-I00 funded by MCIN/AEI/10.13039/501100011033/ and by "ERDF A way of making Europe". It has also received support from the French government under the France 2030 investment plan, as part of the Initiative d'Excellence d'Aix-Marseille Université - A\*MIDEX (AMX-22-RE-AB-157).

## REFERENCES

1. S. Floss, F. Czwielong, M. Kaltenbacher, and S. Becker. Design of an in-duct micro-perforated panel absorber for axial fan noise attenuation. *Acta Acustica*, **5**, 24, 2021.
2. K. Sakagami, K. Toyoda, M. Yairi, and T. Okuzono. Three-dimensional space sound absorbers using microperforated panels. In *Proceedings of the 5th joint meeting of the Acoustical Society of America and the Acoustical Society of Japan*, page 2993. Honolulu, Hawaii, USA, 28 November – 02 December 2016.
3. F. Bucciarelli, G.P. Malfense Fierro, and M. Meo. A multilayer microperforated panel prototype for broadband sound absorption at low frequencies. *Applied Acoustics*, **146**, 134–144, 2019.
4. T. Bravo and C. Maury. Causally-guided acoustic optimization of rigidly-backed micro-perforated partitions: Case studies and experiments. *Journal of Sound and Vibration*, **523**, 116735, 2022.
5. J. Christensen, L. Martinez-Moreno, and F.J. Garcia-Vidal. All-angle blockage of sound by an acoustic double-fishnet metamaterial. *Applied Physics Letters*, **97**, 134106, 2010.

6. J.S. Bell, I.R. Summers, A.R.J. Murray, E. Hendry, J.R. Sambles, and A.P. Hibbins. Low acoustic transmittance through a holey structure. *Physical Review B*, **85**, 214305, 2012.
7. N. Akozbek, N. Mattiucci, M.J. Bloemer, M. Sanghadasa, and G. D'Aguanno. Manipulating the extraordinary acoustic transmission through metamaterial-based acoustic band gap structures. *Applied Physics Letters*, **104**, 161906, 2014.
8. N. Jiménez, V. Romero-García, A. Cebrecos, R. Picó, V.J. Sánchez Morcillos, L.M. García-Raffi. Broadband quasi perfect absorption using chirped multi-layer porous materials. *American Institute of Physics Advances*, **6**, 121605, 2016.
9. V. Romero-García, N. Jiménez, G. Theocharis, V. Achilleos, A. Merkel, O. Richoux, V. Tournat, J.-P. Groby, and V. Pagneux. Design of acoustic metamaterials made of Helmholtz resonators for perfect absorption by using the complex frequency plane. *Comptes Rendus de Physique*, **21**, 713–749, 2020.
10. V. Romero-García, G. Theocharis, O. Richoux, and V. Pagneux. Use of complex frequency plane to design broadband and sub-wavelength absorbers. *Journal of the Acoustical Society of America*, **139**, 3395–3403, 2016.
11. M. Toyoda, R.L. Mu, and D. Takahashi. Relationship between Helmholtz-resonance absorption and panel-type absorption in finite flexible microperforated-panel absorbers. *Applied Acoustics*, **71**, 315–320, 2010.
12. Y. Lee, E.W.M. Lee, and C.F. Ng. Sound absorption of a finite flexible micro-perforated panel backed by an air cavity. *Journal of Sound and Vibration*, **287**, 227–243, 2005.
13. T. Bravo, C. Maury, and C. Pinhede. Enhancing sound absorption and transmission through flexible multi-layer micro-perforated structures. *Journal of the Acoustical Society of America*, **134**, 3363–3373, 2013.
14. J.S. Bolton. The effect of flexibility on the acoustical performance of microperforated materials (A). *Journal of the Acoustical Society of America*, **132**, 1887, 2012.
15. J. Tournadre, M.A. Temiz, P. Martinez-Lera, W. De Roeck, and W. Desmet. Vibro-acoustic response of flexible Micro-Perforated Plates: Impact of the boundary condition at the perforation walls. In *Proceedings of the ISMA 2019*, Leuven, Belgium, 19–20 September 2019.
16. D.Y. Maa. Potential of microperforated panel absorber. *Journal of the Acoustical Society of America*, **104**, 2861–2866 (1998).
17. J. Allard and N. Atalla. *Propagation of Sound in Porous Media: Modelling Sound Absorbing Materials*, 2nd Edition, Wiley, 2009.
18. C. Li, B. Cazzolato, and A. Zander. Acoustic impedance of micro perforated membranes: Velocity continuity condition at the perforation boundary. *Journal of the Acoustical Society of America*, **139**, 93–103 (2016).
19. L. Gallerand, M. Legrand, T. Dupont, and P. Leclaire. Vibration and damping analysis of a thin finite-size microperforated plate. *Journal of Sound and Vibration*, **541**, 117295, 2022.
20. T. Bravo, C. Maury, and C. Pinhède. Sound absorption and transmission through flexible micro-perforated panels backed by an air layer and a thin plate. *Journal of the Acoustical Society of America*, **131**, 3853–3863, 2012.